Semiconductor Physics, Quantum Electronics & Optoelectronics, 2024. V. 27, No 4. P. 427-435.

Semiconductor physics

Theoretical calculations of the properties of the binary compound semiconductor GaSb

B.M. Ahmad, H.T. Abulla, M.N.S. Rammoo

Department of Physics, Faculty of Science, University of Zakho, Kurdistan Region, Iraq
Corresponding author e-mail: bewar.mohammed@uoz.edu.krd

Abstract. Pseudopotentials and density functional theory (DFT) implemented in the ABINIT code were used to study the properties of the GaSb cubic alloy zinc-blende structure. Both the local density approximation and the generalized gradient approximation were used for the exchange-correlation (XC) potential calculation. The calculated lattice parameter aligns well with available experimental and theoretical results. Elastic constants, Young's modulus, shear modulus, and anisotropy factor were determined, and the pressure dependence of elastic constants was investigated. Band gaps were initially calculated but showed discrepancies with experimental values due to the known band gap problem of DFT. To enhance accuracy, the Green function and screened Coulomb interaction approximation were introduced. The impact of thermal effects on compound properties was investigated using the quasi-harmonic Debye model, presenting variations in volume, heat capacities, thermal expansion coefficient, and Debye temperature concerning pressure and temperature.

Keywords: electronic band structure, elastic properties, thermodynamic, band gap energy, density functional theory, local density approximation, general gradient approximation.

https://doi.org/10.15407/spqeo27.04.427
PACS 31.15.A-, 31.15.E-, 63.70.+h, 71.15.Dx

Manuscript received 17.03.24; revised version received 11.07.24; accepted for publication 13.11.24; published online 06.12.24.

1. Introduction

Renewed interest has emerged in gallium and aluminum antimonide due to their potential applications in opto-electronic devices, namely solar cells, photodiodes, and phototransistors, as well as in semiconductor lasers and light-emitting diodes [1–7]. Understanding the properties of semiconductors is crucial for the advancements in computer science and electronics, particularly in the development of barrier materials for high mobility and long-wavelength electronic devices [8–10]. Castano-Gonzalo *et al*. [11] studied the structural and electronic properties of GaSb. This theoretical investigation employed (DFT) using the plane-wave pseudopotential approach. M. Gmitra and J. Fabian [12] used first-principles methodologies tailored to accurately describe semiconductor materials, incorporating a modified Becke–Johnson potential integrated into the exchange-correlation functional. This approach enables us to obtain the electronic band structures for zinc-blende and wurtzite phases of GaAs, GaSb, InAs, and InSb. Caid *et al*. [13] carried out a theoretical investigation of the structural, electronic, and optical characteristics of $(InAs)_m/(GaSb)_n$ superlattices. The authors used the full-potential linear muffin-tin orbital (FP-LMTO) method within the framework of DFT employing the local density approximation (LDA) method. Bengasmia *et al.* [14] performed *ab-initio* calculations to study the structural properties of GaSb in the ground state and under the effect of hydrostatic pressure. The study employed the projected augmented wave pseudo-potentials (PAW) method within the framework of DFT, using the Quantum Espresso code. The exchange-correlation functional was modeled using generalized gradient approximation (GGA). The vibrational, mechanical, and optical properties of GaSb under the influence of temperature have been studied in [15]. Garwood *et al.* [16] demonstrated the potential of first-principles calculations using hybrid DFT to predict band gaps in InAs and GaSb semiconductor superlattices accurately.

Investigating temperature dependences provides valuable insights into the properties of semiconductor optoelectronic and electronic band structures. Different studies have investigated the effects of pressure and temperature on energy gaps in semiconductors [17]. Research on Group III–V semiconductors, particularly gallium antimonide (GaSb) and related semiconductors, has garnered significant interest due to their potential

advantages in optoelectronic applications. GaSb and its counterparts are attractive for their high carrier mobility and narrow band gap (0.75 eV at 300 K) [18], making them promising for high-performance optoelectronic devices in the mid-infrared (IR) spectrum. However, the efficacy of these devices heavily relies on the quality of the crystal structure and emission properties of the materials. Consequently, efforts in research are directed towards improving crystal quality, fine-tuning alloy compositions, and the enhancement of optical properties in GaSb semiconductors. The investigation of thermo-dynamic properties, including entropy *S* serves as a quantification of the multitude of distinct configurations available to a thermodynamic system.

In this study, we focus on how temperature influences the thermodynamic properties of GaSb. In the study, PAW is within the framework of DFT, GGA, and LDA are used for exchange-correlation. In addition, the electronic band structures of GaSb semiconductors are investigated. We predict these effects by analyzing changes in lattice constants, and consequently, thermo-dynamics properties with the variations of temperature. Furthermore, we investigate the influence of pressure on the elastic properties, including elastic constants, bulk modulus, shear modulus, and Young's modulus for the material.

2. Computational method

The Brillouin zone (ZB) unit cell of GaSb involves the placement of the Sb atom at the coordinates (0 0 0) and the Ga atom at the coordinates (0.25 0.25 0.25). Notably, Sb and Ga have atomic numbers 51 and 31, respectively. The electronic configuration for Sb is $1s^2\ 2s^2\ 2p\ 3s^2\ 3p4s^1\ 3d^1\ 4s^2\ 4p\ 5s^2\ 4d^1\ 5p^3$, while Ga electronic configuration is $1s^2\ 2s^2\ 2p\ 3s^2\ 3p\ 4s^2\ 3d^1\ 4p^1$. In this study, pseudo-potentials have been employed, considering Sb with $5s^2$, $5p^3$ as the valence states and Ga with $4s^2$, $4p^1$ [19].

The ABINIT code [20], using the PAW approach within the framework of DFT, has been employed to investigate various properties of the binary compound GaSb. A Monkhorst–Pack grid is selected through convergence studies to achieve *k*-grid sampling in ZB integration. The plane wave kinetic energy cutoff, set at 870.765 eV, is determined through convergence studies on total energy. In the ZB crystal structure, a primitive unit cell is employed in *ab-initio* calculations for the GaSb compound. The investigation of thermodynamic properties is carried out using the quasi-harmonic Debye model, implemented within the Gibbs program [21].

3. Results

3.1. Structural properties

The lattice constant (*a*) for ZB-GaSb was determined by applying both LDA and GGA methods, involving the calculation of total energy E_{TOT} within a range of diverse values. The resulting plot, depicted in Fig. 1, displays the relationship between E_{TOT} and the corresponding *a* value. The equilibrium *a*, representing the minimum energy state, was identified by selecting the value of *a* associated with the lowest minimum energy on the plot.

Table 1. Calculated lattice constant (*a*) for the ZB of GaSb compound.

Present work		Other works	
LDA	GGA	LDA	GGA
6.043	6.233	5.981 [11]	6.219 [11]
		6.053 [22]	6.219 [22]

The GGA calculations used an equilibrium *a* of 6.233 Å for GaSb, whereas in the LDA calculations, it was determined to be 6.043 Å. These *a* values are presented in Table 1, alongside results from other theoretical studies and experimental data. It is worth noting that the obtained results demonstrate a satisfactory agreement with both theoretical and experimental values, particularly with LDA calculations showing a better fit.

3.2. Band structure and energy gap

The band structures and band gap energies have been determined by calculations employing both LDA and GGA methods. GaSb, as a material, exhibits a direct band gap. The electronic band structure of GaSb along high symmetry directions is illustrated in Fig. 2.

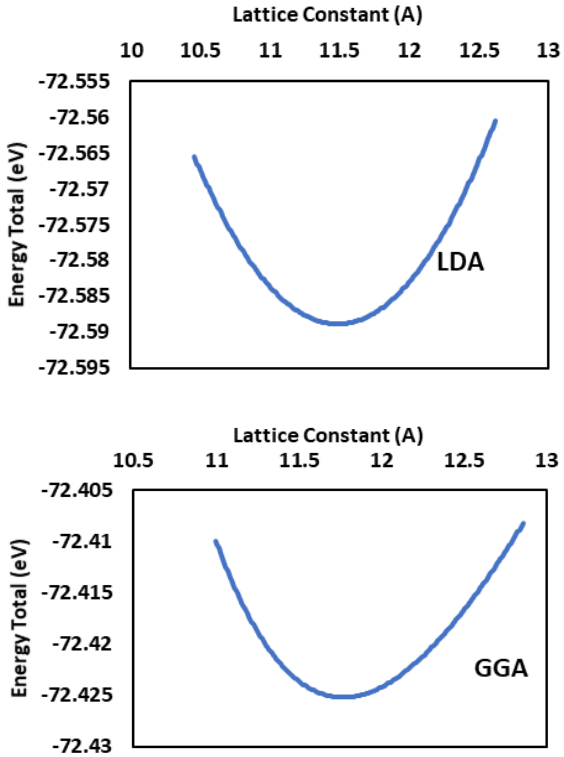

Fig. 1. The variation of total energy *vs* lattice constant for the ZB crystal structure of GaSb calculated using the LDA and GGA methods. For interpretation of the colors in the figure(s), the reader is referred to the web version of this article.

Table 2. Calculated using LDA, GGA, and GW energy band gap (eV) in the Γ symmetry point of GaSb.

Present work			Experimental	Other works		
LDA	GGA	GW	0.82 [23]	LDA	GGA	GW
0.002	0.00	0.802		0.00 [22]	0.02 [22]	0.85 [24]

A summary of the compound band gap values is presented in Table 2, comparing the computed results with experimental and other theoretical values. One can see a good agreement of our results with other theoretical ones. In this instance, the outcomes obtained using GGA and LDA calculations deviate significantly from the experimental values. This discrepancy is particularly notable in the context of extended systems, namely, bulk semiconductors and insulators.

The widely employed DFT method tends to outcome band gaps that are considerably smaller than observed experimentally. In addition, in specific cases, it may even give an incorrect band order. A primary strategy to address this issue involves employing Hedin's Green function and screened Coulomb interaction (GW) approximation. In this approach, an energy-dependent, nonlocal self-energy is introduced as a replacement for LDA in the exchange-correlation energy. The true quasi-particle eigenvalues are subsequently determined by correcting the LDA eigenvalues through perturbation theory.

The outcomes for the compound, considering GW, along with experimental and various theoretical results, are presented in Table 2. As evident from the table, the GW approximations outcome more accurate results for the energy band gap compared to Kohn–Sham LDA or GGA. This involves a correction to the Kohn–Sham LDA and GGA band gaps.

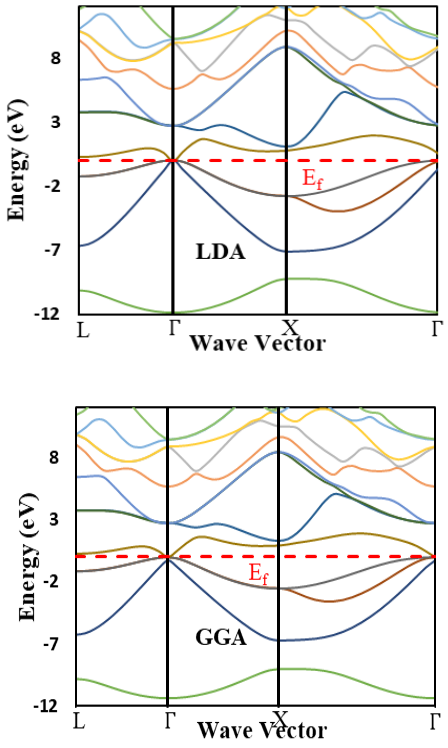

Fig. 2. The Kohn–Sham electronic band structure for the ZB-GaSb calculated using the LDA and GGA methods.

3.3. Elastic properties

The study of elastic properties of materials under various pressures enhances our comprehension of fundamental physical principles, encompassing interatomic forces, mechanical characteristics, phase transitions, and more. The elastic constants of solids establish a connection between the mechanical and dynamic traits of crystals, offering crucial insights into the forces acting within solids. Notably, in cubic crystals, there are only three distinct elastic constants, namely C_{11}, C_{12}, and C_{44}.

Table 3 presents calculated elastic constant values for the GaSb compound in the cubic zinc-blende structure. Additionally, the table includes values from experimental and alternative theoretical studies for each elastic constant. In this study, the results for C_{11}, C_{12}, and C_{44} demonstrate a strong concurrence with other theoretical models and experimental findings, particularly indicating favorable alignment with the results obtained through LDA. The conventional criteria for mechanical stability in cubic crystals involves the elastic constants, specifically $C_{11} - C_{12} > 0$, $C_{11} > 0$, $C_{44} > 0$, $C_{11} + 2C_{12} > 0$, and $C_{12} < B < C_{11}$. Upon study of the elastic constants presented in Table 3 for the GaSb compound, it is evident that these stability conditions are met in the ZB structure. This observation indicates that the compound exists in a mechanically stable state at zero pressure. The Zener anisotropy factor $A = \frac{2C_{44}}{C_{11} - C_{12}}$ serves as a measure of the extent of elastic anisotropy exhibited by a crystal. In the case of a fully isotropic material, the factor A assumes a value of 1. The calculation of factor A is based on the computed data, and this relationship is utilized to determine its value [27].

Table 3. Elastic constants of GaSb calculated using LDA and GGA under zero pressure.

Present work			Experiment	Other works
GaSb	GGA	LDA		
C_{11}	71.5	87	88.34 [25]	89.8 [26]
C_{12}	30.5	37.9	40.23 [25]	38.7 [26]
C_{44}	36	43.0	43.22 [25]	41.5 [26]

Table 4. The obtained bulk modulus, shear modulus, Young's modulus *E*, Pugh's modulus ratio, Zener's anisotropy factor, and Poisson's ratio *v* (in GPa) for the ZB structure of the GaSb compound.

Present work	*B*	*G*	*E*	*G*/*B*	*A*	*v*
LDA	55.15	34.34	85.31	0.622	1.751	0.242
GGA	46.5	28.72	71.45	0.617	1.756	0.244
Other works	55.8 [26]					

The Zener anisotropy factor *A*, Poisson's ratio *v*, shear modulus *G*, Young's modulus *E*, and the inverse Pugh's modulus ratio *G*/*B* have been computed and are presented in a concise form in Table 4 *via* the following relations:

$$v = \frac{1}{2}\left[\frac{B-\frac{2}{3}G}{B+\frac{1}{3}G}\right], \quad (2)$$

$$E = \frac{9GB}{G+3B}. \quad (3)$$

The observed *A* values exceeding 1.0 indicate that GaSb cannot be considered elastically isotropic. Particularly crucial for practical applications *v*, *G*, and *E* are frequently measured in the study of hardness for polycrystalline materials. These elastic properties are derived from the computed data using specific mathematical relations. The physical significance of these properties lies in their reflection of the material response to mechanical stress and deformation. *v* relates to lateral and axial strains, *G* measures a material resistance to deformation under shear stress, and *E* quantifies its resistance to linear deformation *via* the following relations:

$$G_V = \frac{C_{11}-C_{12}+3C_{44}}{5}, \quad (4)$$

$$\frac{5}{G_R} = \frac{4}{C_{11}-C_{12}} + \frac{3}{C_{44}}, \quad (5)$$

where

$$G = (G_V + G_R)/2. \quad (6)$$

G characterizes a material resistance to plastic deformation, while *B* represents its resistance to fracture. S.F. Pugh introduced *G*/*B* in polycrystalline phases as a predictor of material brittleness or ductility. A higher (lower) *G*/*B* value indicates ductility (brittleness). The critical threshold that separates ductile from brittle behavior is typically close to 0.5. Analyzing the calculated *G*/*B* values in Table 4, it is evident that GaSb is ductile, as the *G*/*B* ratio exceeds 0.5. *v* offers valuable insights into the nature of bonding forces, more so than other elastic constants. Typically falling within 0.25…0.5, *v* is a crucial indicator. The calculated *v* in this case is close to 0.25, suggesting that the material primarily possesses central interatomic forces [27]. A larger *v* indicates an enhanced plasticity, emphasizing the material ability to undergo deformation under applied stress.

After determining elastic constants at zero pressure, calculations were performed for various pressures ranging from 1 to 12 GPa for GaSb, employing both LDA and GGA methods. Fig. 3 visually represents the changes in the three elastic constants throughout these pressure variations in both LDA and GGA calculations. As anticipated, the graphs indicate that the values of C_{11} and C_{12} consistently exhibit positive trends, increasing linearly with pressure. At the same time, C_{44} experiences a weak dependence on the pressure (the changes of C_{44} do not exceed error bars).

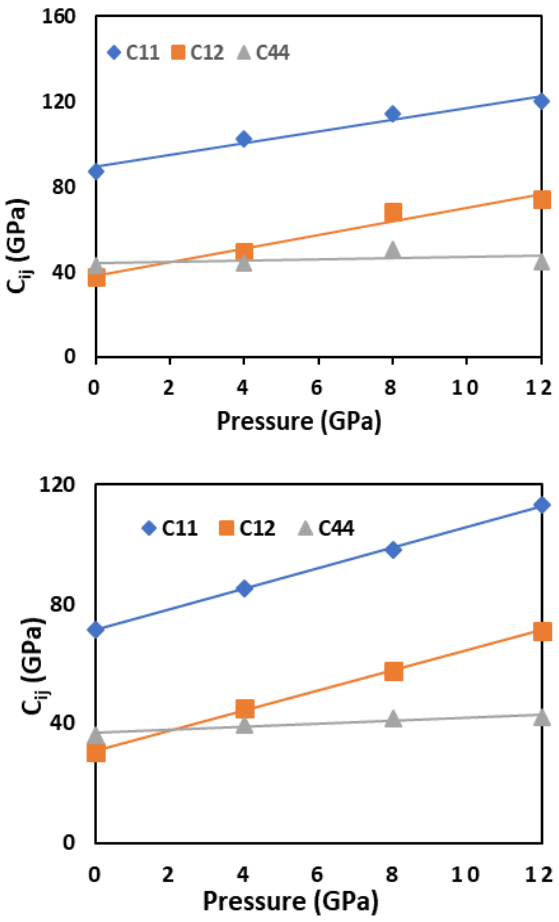

Fig. 3. Pressure dependences of C_{ij} for GaSb in ZB structure plotted using the results of LDA and GGA calculations.

3.4. Thermodynamic properties

The field of thermodynamics originates from the investigation of two distinct forms of energy transfer, namely, heat and work, and their connection to the macroscopic variables of a system, including volume, pressure, and temperature. To investigate the thermodynamic characteristics of the GaSb compound under elevated temperature and pressure conditions, the quasi-harmonic Debye model has been employed. In this model, the non-equilibrium Gibbs function, denoted as G^* (V; P, T), is expressed in the following relation [21]:

$$G^*(V:P,T)=E(V)+A_{vib}[\theta(V):T]. \quad (7)$$

The use of the quasi-harmonic Debye model makes it feasible to ascertain the thermodynamic properties of compounds at various temperatures and pressures based on the computed energy-volume (E-V) data at T = 0 and P = 0. In this study, we have investigated the thermodynamic parameters for the studied compound through GGA calculations. Fig. 4 illustrates the changes in the bulk modulus of the GaSb compound with temperature under pressures of 0, 10, and 15 GPa. One can see that under constant temperature, the bulk modulus B demonstrates an increase with rising pressure, whereas, under constant pressure, B decreases as the temperature rises. Additionally, it is noteworthy that the temperature dependence of the bulk modulus is minimal at elevated temperatures. The findings concerning the bulk modulus suggest a parallel effect between increasing pressure and decreasing temperature on the GaSb material. This observation has implications for various applications, particularly in materials science and engineering. Understanding how pressure and temperature influence the bulk modulus is crucial for predicting and optimizing the mechanical behavior of materials under different conditions, which is essential in the design and manufacturing of materials for specific applications, namely for high-pressure and high-temperature environments. These insights contribute to the broadening of the field of material science and provide valuable information for the development of advanced materials with tailored properties.

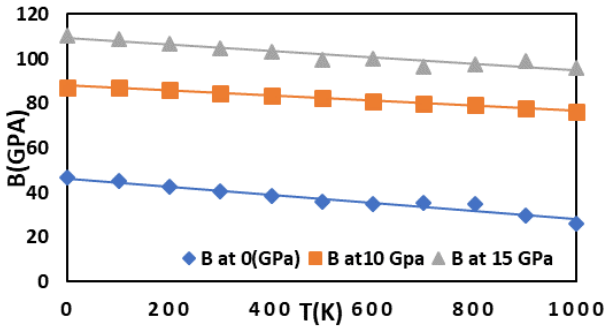

Fig. 4. Temperature dependences of the bulk modulus at the pressures 0, 10, and 15 GPa calculated for the ZB–GaSb.

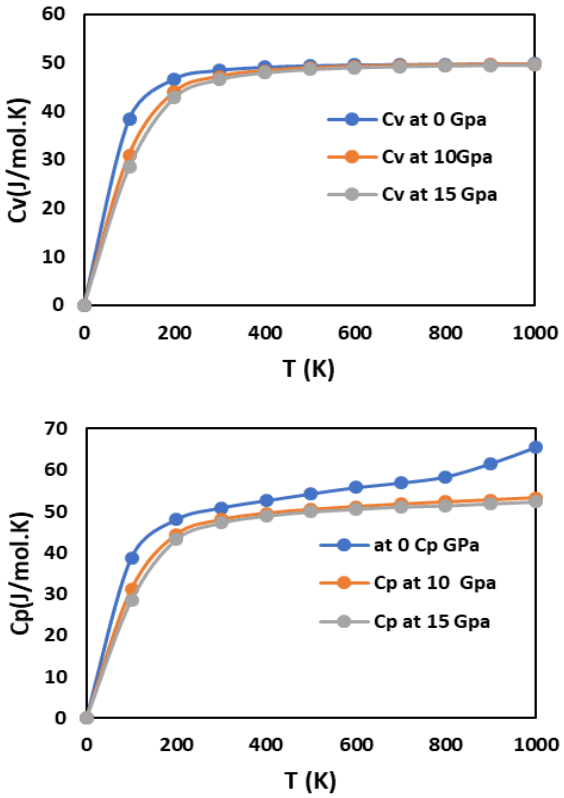

Fig. 5. Variation of the heat capacities C_V and C_P with the temperature at different pressures for ZB–GaSb calculated using the GGA method.

The study delves into exploring the heat capacity at constant pressure C_P and constant volume C_V concerning temperature, within the pressure range 0…5 GPa for the GaSb compound. Fig. 5 illustrates the temperature-dependent variations of C_V and C_P in GGA calculations. One can see that at elevated temperatures, the constant volume heat capacity C_V tends towards the Petit and Dulong limit, a characteristic shared by all solids.

This limit represents a plateau where the heat capacity reaches its maximum value due to the contribution of all vibrational modes in the solid. Conversely, at sufficiently low temperatures, C_V behaves proportionally to T^3, reflecting the dominance of low-energy vibrational modes [28].

It is noteworthy that at intermediate temperatures, the temperature dependence of C_V is intricately influenced by the specifics of atomic vibrations. Traditionally, these mode characteristics were solely determined through experimental means. This information contributes significantly to our understanding of the thermal behavior of materials, particularly under high-pressure conditions. This property is beneficial in various applications, particularly in thermal management and engineering, as it signifies that beyond a certain temperature threshold close to 200 K, the substance heat capacity remains relatively constant. This stability simplifies predictions and facilitates more effective control of temperature-related processes and systems.

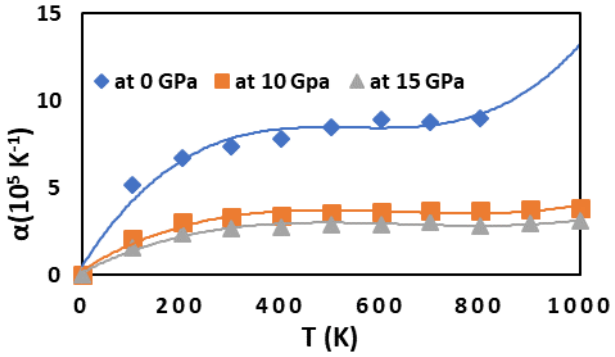

Fig. 6. Variation of the thermal expansion coefficient α as a function of temperature at the pressures 0, 10, and 15 GPa for ZB-GaSb compound calculated using the GGA method.

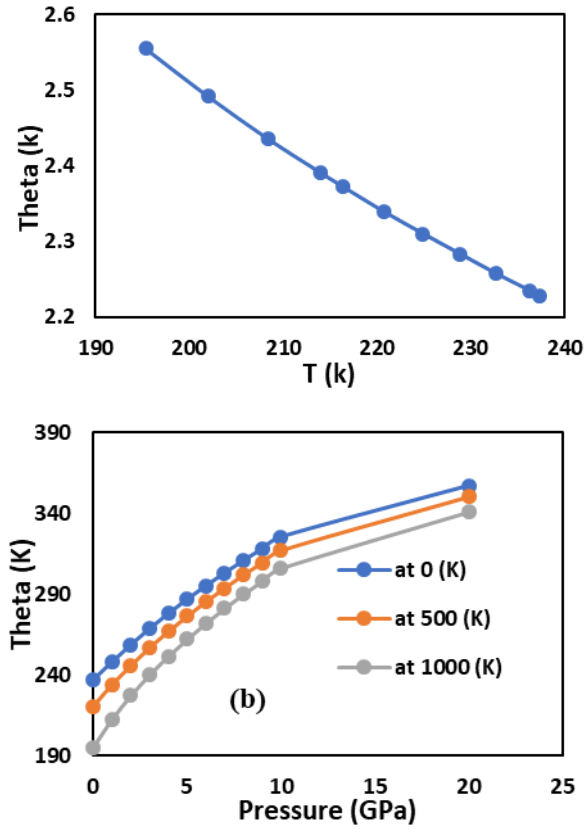

Fig. 7. Variation of the Debye temperature *vs* temperature (a) and pressure (b) for ZB-GaSb calculated using the GGA method.

Solids typically undergo expansion when subjected to heating and contraction when cooled. The value of this expansion, measured as the ratio of the change in size to the change in temperature, is termed the material coefficient of thermal expansion (α), and it generally exhibits variation with temperature. Fig. 6 depicts the coefficient α as a function of temperature and pressure in GGA calculations. Following a pronounced increase, particularly up to 200 K, attributed to electronic contributions, α of the compounds stabilizes and maintains a relatively constant value between 200 and 1000 K.

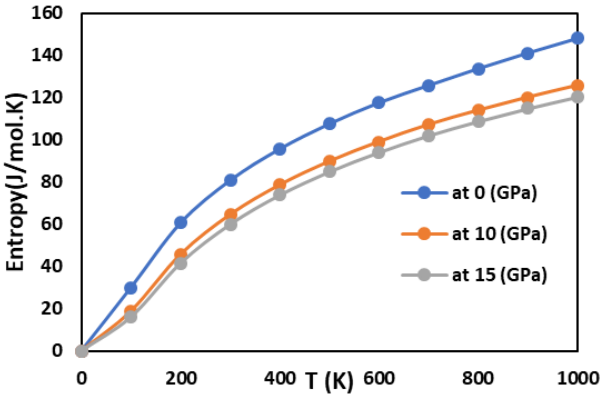

Fig. 8. Entropy versus temperature at different pressures for ZB-GaSb calculated using the GGA method.

In the context of the Debye theory, The Debye temperature represents the highest frequency of vibrational modes in a crystal, which signifies the upper limit of thermal excitations in the material. Fig. 7 illustrates the dependence of the Debye temperature on temperature at zero pressure for GaSb compound, while Fig. 7 depicts its variation with pressure at fixed temperatures, specifically through GGA calculations. It is noteworthy that the Debye temperature remains relatively constant within the range of 196 to 200 K and exhibits a quadratic decrease with increasing temperature for $T > 190$ K. Additionally, under constant temperature conditions, the Debye temperature demonstrates a linear increase in response to applied pressure. The increase in Debye temperature with pressure is due to the compression of the crystal lattice, which stiffens the bonds between atoms and increases the frequencies of the vibrational modes. This effect is consistent with the behavior seen in other semiconductors and can be explained through a combination of phonon theory and elasticity.

These unique characteristics of GaSb Debye temperature have practical implications in various applications: such as thermal management in electronics [30], acoustic and thermal wave devices [31], opto-electronic devices [32] for harsh environments [29].

It is frequently interpreted as a level of randomness or the degree to which the system advances toward achieving thermodynamic equilibrium. Fig. 8 indicates a clear trend as pressure increases, S decreases, suggesting that the compound is well-suited for optoelectronic devices with improved electronic transport properties [33]. To the best of the author's knowledge, this research is the first theoretical investigation [29] of the elastic constants (C_{11}, C_{12} and C_{44}) with pressure and entropy (S) and *expansion coefficient* (α) with temperature.

Thermodynamic properties are important due to the stability of crystal structures. Thermodynamic properties such as enthalpy and free energy can provide information about the stability of the zinc-blende structure under different conditions, such as, temperature and pressure. This can help in determining the conditions under which zinc-blende is the most stable phase.

4. Conclusions

In this study, the thermodynamic properties under the influence of temperature and the elastic properties under pressure of GaSb were investigated. The determined lattice parameters and the bulk modulus of GaSb closely match experimental data, with the LDA method providing more accurate values, especially for the lattice constant and bulk modulus. In contrast, GGA yields more precise results for these properties. E_g computed using LDA and GGA shows inaccuracies when compared to experimental values, attributed to the inherent band gap problem of DFT. However, implementing the GW approximation, better result of E_g was obtained compared to the available practical values. Elastic constants of GaSb were calculated by LDA. The results of LDA were in reasonable agreement with the experimental results compared to the obtained values by GGA. The elastic constants of GaSb confirm its mechanical stability and suitability for high-pressure applications, making it valuable for use in various electronic and optoelectronic devices. Although the elastic behavior of GaSb is similar to other semiconductors, the specific values of its bulk modulus and *G*/*B* ratio are important for its stability and ductility under pressure. These characteristics make GaSb particularly suitable for optoelectronic devices in high-stress environments, where both flexibility and durability are critical. At high temperatures, the heat capacity C_V of solids approaches the Dulong–Petit limit. The Debye temperature θ_D remains nearly constant from 196 to 200 K, decreasing quadratically beyond 200 K, and increases linearly with pressure at constant temperature. In addition, entropy shows minimal sensitivity to pressure changes, underscoring the stability of vibrational modes across varying pressures.

Acknowledgments

The author expresses gratitude to the University of Zakho and the Physics Department for their support in completing this work.

Conflict of interest

The authors declare that there is no conflict of interest regarding the publication of this manuscript.

References

1. Ermolaev M., Lin Y., Shterengas L. *et al*. GaSb-based type-I quantum well 3–3.5-μm cascade light emitting diodes. *IEEE Photonics Technol. Lett.* 2018. **30**, No 9. P. 869–72. https://doi.org/10.1109/LPT.2018.2822621.
2. Haddadi A., Adhikary S., Dehzangi A., Razeghi M. Mid-wavelength infrared heterojunction phototransistors based on type-II InAs/AlSb/GaSb superlattices. *Appl. Phys. Lett.* 2016. **109**, No 2. P. 021107. https://doi.org/10.1063/1.4958715.
3. Wun J.M., Wang Y.W., Chen Y.H. *et al*. GaSb-based *p-i-n* photodiodes with partially depleted absorbers for high-speed and high-power performance at 2.5-μm wavelength. *IEEE Trans. Electron. Devices.* 2016. **63**, No 7. P. 2796–2801. https://doi.org/10.1109/TED.2016.2561202.
4. Nguyen T.D., Kim J.O., Lee S.J. Growth of InGaAsSb/GaSb compound for infrared optoelectronic devices. *Condensed Matter and Interphases*. 2022. **24**, No 2. P. 250–255. https://doi.org/10.17308/kcmf.2022.24/9265.
5. Vadiee E., Fang Y., Zhang C. *et al*. Temperature dependence of GaSb and AlGaSb solar cells. *Curr. Appl. Phys.* 2018. **18**, No 6. P. 752–761. https://doi.org/10.1016/j.cap.2018.03.007.
6. Delorme O., Cerutti L., Luna E. *et al*. GaSbBi/GaSb quantum well laser diodes. *Appl. Phys. Lett.* 2017. **110**, No 22. P. 222106. https://doi.org/10.1063/1.4984799.
7. Lumb M.P., Mack S., Schmieder K.J. *et al*. GaSb-based solar cells for full solar spectrum energy harvesting. *Adv. Energy Mater.* 2017. **7**, No 20. P. 1700345. https://doi.org/10.1002/aenm.201700345.
8. Lee J.S., Shojaei B., Pendharkar M. *et al*. Contribution of top barrier materials to high mobility in near-surface InAs quantum wells grown on GaSb (001). *Phys. Rev. Mater.* 2019. **3**, No 1. P. 014603. https://doi.org/10.1103/PhysRevMaterials.3.014603.
9. Teng Y., Zhao Y., Wu Q. *et al*. High-performance long-wavelength InAs/GaSb superlattice detectors grown by MOCVD. *IEEE Photonics Technol. Lett.* 2018. **31**, No 2. P. 185–188. https://doi.org/10.1109/LPT.2018.2889575.
10. Thomas C., Hatke A.T., Tuaz A. *et al*. High-mobility InAs 2DEGs on GaSb substrates: A platform for mesoscopic quantum transport. *Phys. Rev. Mater.* 2018. **2**, No 10. P. 104602. https://doi.org/10.1103/PhysRevMaterials.2.104602.
11. Castaño-González E.E., Seña N., Mendoza-Estrada V. *et al*. First-principles calculations of the electronic and structural properties of GaSb. *Semiconductors*. 2016. **50**. P. 1280–1286. https://doi.org/10.1134/S1063782616100110.
12. Gmitra M., Fabian J. First-principles studies of orbital and spin-orbit properties of GaAs, GaSb, InAs, and InSb zinc-blende and wurtzite semiconductors. *Phys. Rev. B*. 2016. **94**, No 16. P. 165202. https://doi.org/10.1103/PhysRevB.94.165202.
13. Caid M., Rached D., Cheref O. *et al*. Full potential study of the structural, electronic and optical properties of $(InAs)_m/(GaSb)_n$ superlattices. *Comput. Condens. Matter*. 2019. **21**. P. e00394. https://doi.org/10.1016/j.cocom.2019.e00394.
14. Bengasmia F., Benamrani A., Boutahar L. *et al*. Hydrostatic pressure effect on the structural parameters of GaSb semiconducting material: Ab-initio calculations. *J. Phys. Chem. Res.* 2022. **1**, No 2. P. 25–30. https://doi.org/10.58452/jpcr.v1i2.24.
15. Al Maaitah I.F. Mechanical, optical, and lattice vibrational properties of gallium antimonide (GaSb) semiconductor under the influence of temperature. *Phys. Scr*. 2023. **98**, No 5. P. 055904. https://doi.org/10.1088/1402-4896/acc76c.

16. Garwood T., Modine N.A., Krishna S. Electronic structure modeling of InAs/GaSb superlattices with hybrid density functional theory. *Infrared Phys. Techn.* 2017. **81**. P. 27–31. https://doi.org/10.1016/j.infrared.2016.12.007.
17. Elkenany E.B. Theoretical investigations of electronic, optical and mechanical properties for GaSb and AlSb semiconductors under the influence of temperature. *Spectrochim. Acta A. Mol. Biomol. Spectrosc.* 2015. **150**. P. 15–20. https://doi.org/10.1016/j.saa.2015.05.033.
18. Niu S., Wei Z., Fang X. *et al*. Brief review of epitaxy and emission properties of GaSb and related semiconductors. *Crystals*. 2017. **7**, No 11. P. 337. https://doi.org/10.3390/cryst7110337.
19. Goedecker S., Teter M., Hutter J. Separable dual-space Gaussian pseudopotentials. *Phys. Rev. B.* 1996. **54**, No 3. P. 1703. https://doi.org/10.1103/PhysRevB.54.1703.
20. Gonze X., Jollet F., Araujo F.A. *et al*. Recent developments in the ABINIT software package. *Comput. Phys. Commun.* 2016. **205**. P. 106–131. https://doi.org/10.1016/j.cpc.2016.04.003.
21. Blanco M.A., Francisco E., Luaña V. GIBBS*:* isothermal-isobaric thermodynamics of solids from energy curves using a quasi-harmonic Debye model. *Comput. Phys. Commun.* 2004. **158**, No 1. P. 57–72. https://doi.org/10.1016/j.comphy.2003.12.001.
22. Ahmed R., Hashemifar S.J., Rashid H., Akbarzadeh H. Physical properties of III-antiminodes – a first principles study. *Commun. Theor. Phys*. 2009. **52**, No 3. P. 527. https://doi.org/10.1088/0253-6102/52/3/28.
23. Varshni Y.P. Temperature dependence of the energy gap in semiconductors. *physica*. 1967. **34**, No 1. P. 149 –154. https://doi.org/10.1016/0031-8914(67)90062-6.
24. Kim Y.S., Marsman M., Kresse G. *et al.* Towards efficient band structure and effective mass calculations for III-V direct band-gap semiconductors. *Phys. Rev. B*. 2010. **82**, No 20. P. 205212. https://doi.org/10.1103/PhysRevB.82.205212.
25. Azuhata T., Sota T., Suzuki K. Elastic constants of III-V compound semiconductors: modification of Keyes' relation. *J. Phys.: Condens. Matter*. 1996. **8**, No 18. P. 3111. https://doi.org/10.1088/0953-8984/8/18/005.
26. Vyas P.S., Thakore B.Y., Gajjar P.N., Jani A.R. On the elastic constants of $Ga_xIn_{1-x}Sb$ semiconductor. *AIP Conf. Proc. American Institute of Physics*. 2010. https://doi.org/10.1063/1.3530552.
27. Nye J.F. *Physical Properties of Crystals: Their Representation by Tensors and Matrices.* Oxford University Press, 1985.
28. Debye P. On the Theory of Specific Heats. *Annalen der Physik.* 1912. **39**. P. 789–839. http://dx.doi.org/10.1002/andp.19123441404.
29. Baloğlu E.C., Ustunel H., Dal H. Temperature-dependent thermoelastic properties of GaSb and InSb semiconductors: Identification through ab initio DFT simulations. *Phys. B: Condens. Matter*. 2022. **643**. P. 414135. https://doi.org/10.1016/j.physb.2022.414135.
30. Perez J.-P., Laurain A., Cerutti L. *et al.*. Technologies for thermal management of mid-IR Sb-based surface emitting lasers. *Semicond. Sci. Technology*. 2010. **25**, No 4. P. 045021. https://doi.org/10.1088/0268-1242/25/4/045021.
31. Othmani C., Takali F., Njeh A., Ben Ghozlen M.H. Study of the influence of semiconductor material parameters on acoustic wave propagation modes in GaSb/AlSb bi-layered structures by Legendre polynomial method. *Phys. B: Condens. Matter*. 2016. **496**. P. 82–91. https://doi.org/10.1016/J.PHYSB.2016.05.030.
32. Guo Baozeng. Properties, preparation and applications of GaSb. *Semiconductor Optoelectronics*. 1999; Shi J., Yang C., Chen Y. *et al*. Thermal characterization of high-power GaSb-based laser. *Proc. SPIE.* 2022. **12311. Semiconductor Lasers and Applications XII**. P. 123110R. https://doi.org/10.1117/12.2642099.
33. Bouarissa N. Exciton properties, optical phonon modes, polaron characteristics and plasma frequency of GaSb upon compression. *Mater. Sci. Semicond. Proc.* 2022. **147**. P. 106694. https://doi.org/10.1016/j.mssp.2022.106694.

Authors and CV

Bewar M. Ahmad, born in 1984, defended his Ph.D. thesis in Theoretical Physics in 2023 at the Department of Physics, Faculty of Science, University of Zakho, Kurdistan Region, Iraq. Authored over 3 publications. The area of his scientific interests includes physics and technology of semiconductor materials, hetero and hybrid structures and devices (solar cells, photoresistors, light-emitted structures *etc*.).
https://orcid.org/0009-0008-4714-4913

Hameed T. Abdulla, born in 1987, defended his Ph.D. thesis in Theoretical Physics in 2023 at the Department of Physics, Faculty of Science, University of Zakho, Kurdistan Region, Iraq. Authored over 3 publications. The area of his scientific interests includes physics and technology of semiconductor materials, hetero and hybrid structures and devices (solar cells, photoresistors, light-emitted structures *etc*.).
E-mail: hameed.abdulla@uoz.edu.krd,
https://orcid.org/0000-0001-8490-1057

Mohammed Noor S. Rammoo, born in 1990, defended his MSc. thesis in Quantum Mechanics in 2014 at the Eastern Mediterranean University. Currently he works at the Department of Physics, Faculty of Science, University of Zakho, Kurdistan Region, Iraq. Authored over 3 publications. The area of his scientific interests includes physics and technology of semiconductor materials, hetero and hybrid structures and devices (solar cells, photoresistors, light-emitted structures *etc*.). https://orcid.org/0000-0002-1796-723X, e-mail: mohammed.noor@uoz.edu.krd

Authors' contributions

Ahmad B.M.: conceptualization, data curation, formal analysis, software, resources, project administration, methodology.

Abulla H.T.: formal analysis, funding acquisition, investigation, visualization, writing – original draft preparation, writing – review & editing.

Rammoo M.N.S.: funding acquisition, supervision, validation, writing – original draft preparation, writing – review & editing.

Теоретичні розрахунки властивостей бінарного напівпровідника GaSb

B.M. Ahmad, H.T. Abulla, M.N.S. Rammoo

Анотація. Псевдопотенціали та теорія функціонала густини (DFT), вбудовані в коді ABINIT, було використано для вивчення властивостей структури цинкової обманки кубічного сплаву GaSb. Для розрахунку обмінно-кореляційного потенціалу використано як наближення локальної густини, так і узагальнене градієнтне наближення. Розрахований параметр решітки добре узгоджується з наявними експериментальними та теоретичними результатами. Було визначено пружні константи, модуль Юнга, модуль зсуву та фактор анізотропії, а також досліджено залежність пружних констант від тиску. Спочатку було розраховано заборонені зони, але вони показали розбіжності з експериментальними значеннями через відому проблему забороненої зони DFT. Для підвищення точності було введено функцію Гріна та наближення екранованої кулонівської взаємодії. Вплив теплових ефектів на властивості сполуки було досліджено з використанням квазігармонічної моделі Дебая, що представляє зміни обсягу, теплоємності, коефіцієнта теплового розширення та температури Дебая з урахуванням тиску та температури.

Ключові слова: електронна зонна структура, пружні властивості, термодинаміка, енергія забороненої зони, теорія функціонала густини, апроксимація локальної густини, апроксимація загального градієнта.